AIP | Applied Physics Letters

Optical critical coupling into highly confining metal-insulator-metal resonators

J.-M. Manceau, S. Zanotto, I. Sagnes, G. Beaudoin, and R. Colombelli

Citation: Appl. Phys. Lett. **103**, 091110 (2013); doi: 10.1063/1.4819491
View online: http://dx.doi.org/10.1063/1.4819491
View Table of Contents: http://apl.aip.org/resource/1/APPLAB/v103/i9
Published by the AIP Publishing LLC.

Optical critical coupling into highly confining metal-insulator-metal resonators

J.-M. Manceau,[1,a)] S. Zanotto,[2] I. Sagnes,[3] G. Beaudoin,[3] and R. Colombelli[1,b)]
[1]*Institut d'Electronique Fondamentale, Univ. Paris Sud, UMR8622 CNRS, 91405 Orsay, France*
[2]*NEST, Istituto Nanoscienze—CNR and Scuola Normale Superiore, Piazza San Silvestro 12, 56127 Pisa, Italy*
[3]*Laboratoire de Photonique et Nanostructures, CNRS UPR20, 91460 Marcoussis, France*

(Received 10 July 2013; accepted 13 August 2013; published online 29 August 2013)

We demonstrate controlled optical critical coupling into highly confining metal-insulator-metal grating-based resonators. We achieve the coupling—and hence the absorption—of more than 95% of the incoming photons in a gallium arsenide based system confined between a metallic ground plane and a metallic grating. The demonstration is given in the terahertz range of the electromagnetic spectrum, at $75\,\mu m \leq \lambda \leq 120\,\mu m$, for a semiconductor core thickness of only $10\,\mu m$. It is valid, however, at any wavelength, upon linear scaling. The critical coupling regime is judiciously tuned by precise etching of the semiconductor material in between the metallic fingers. The experimental results are in accordance with the universal behaviour predicted by temporal coupled mode theory. © *2013 AIP Publishing LLC*. [http://dx.doi.org/10.1063/1.4819491]

Critical coupling is the situation when energy is fed to a system with maximum efficiency.[1] In the ideal case, no energy is back-reflected or transmitted. It is a general concept which finds applications in a vast range of fields, such as—to name a few—microwaves and antenna theory, electro technical applications, photonics. It is a crucial property of waveguides coupled to resonators: when the resonator losses equal the coupling constant, the energy transfer is maximal.[2–4] As a corollary, the transmission/reflection via the waveguide drops to zero if there is no mode-coupling.[5] If we remove the waveguide, the concept still applies (freely propagating photons can be reflected or transmitted through the resonator system) and it acquires even greater generality.[6] This concept can have a major impact in the semiconductor field where a detector or a photovoltaic active core can for instance be inserted in such a system:[7–9] maximum efficiency is achieved at critical coupling, since all the energy is dissipated in the resonator. Another field which could benefit from the critical coupling concept is the research domain on perfect absorbers.[10–12] In such systems, at specific frequency and/or angles, most of the impinging radiation is absorbed. While rarely mentioned, almost always such a behaviour can be interpreted in terms of critical coupling condition. This makes a direct link with the recent efforts which are devoted to the development of thermal narrow-band sources[13–16] in which critical coupling can greatly enhance the emission efficiency.

Terahertz (THz) resonators usually employ metallic waveguides and mirrors which enable sub-wavelength confinement in at least one direction.[17,18] For instance, patch cavities with thickness around one micron or less in general exhibit a good coupling efficiency.[19] When dealing instead with thicker THz optical resonators—which are well suited to devices given the reduced level of ohmic losses—the onset of the dispersive regime implies that critical coupling between the incoming light and the resonating modes is not a trivial task. Indeed for such dispersive cavities ($10\,\mu m$ thick), the tight lateral confinement of the resonances is lost and the coupling efficiency drops to lower values. In this letter, we demonstrate an approach which permits to easily tune such dispersive cavities into the critical coupling regime, hence achieving almost total light funnelling into the system which remains highly confined in the vertical dimension. Most of the energy is dissipated in the active core, with a marginal amount of power lost in ohmic losses. We also demonstrate that a simple analysis with temporal coupled mode theory (TCMT) provides a universal behaviour as a function of the coupling parameter.

The studied THz resonator consists of the most commonly used architecture, i.e., a metal-insulator-metal structure as depicted in Figure 1(a). The bottom mirror is a planar gold layer, 1-μm-thick, obtained using a thermo-compressive Au-Au wafer bonding process.[20] The insulator is $10\,\mu m$ thick and is constituted of a 9-μm-thick semi-insulating (SI) GaAs slab, with an extra 1-μm-thick layer of GaAs n-doped to $2.6 \times 10^{18}\,cm^{-3}$. This layer mimics an active region, e.g., a detector via its absorption losses γ_{AR}. If we define as γ_{ohmic} the waveguide losses related to the metallic layers, the non-radiative loss rate γ_{NR} is equal to $\gamma_{AR} + \gamma_{ohmic}$. The system is coupled to the external world with a top 1-D metallic grating (Ti/Au, 5/200 nm, followed by a thin Cr layer for induced coupled plasma (ICP) masking purposes), with period Λ and filling factor ff. Several periods ($\Lambda = 25,\ 30\,\mu m$) and ff (43%, 73%, 77%, 80%) have been implemented. Figure 1(b) presents a scanning electronic microscope (SEM) image of the device with a period of $30\,\mu m$ and ff = 77%. The inset of Figure 1(b) shows the calculated resonant electric field intensity ($|E_z|^2$) in one unit cell of the photonic crystal. The electric field is mainly concentrated at the bottom of the resonator which justifies our choice for the location of the absorbing layer. Referring to Figure 2(a) and the analysis with TCMT, critical coupling is achieved when the radiative (γ_R) and non-radiative (γ_{NR}) loss rates are equal. Here, γ is defined as ν/Q, where Q is a quality factor and ν is the frequency.

a)Email: jean-michel.manceau@u-psud.fr
b)Email: raffaele.colombelli@u-psud.fr

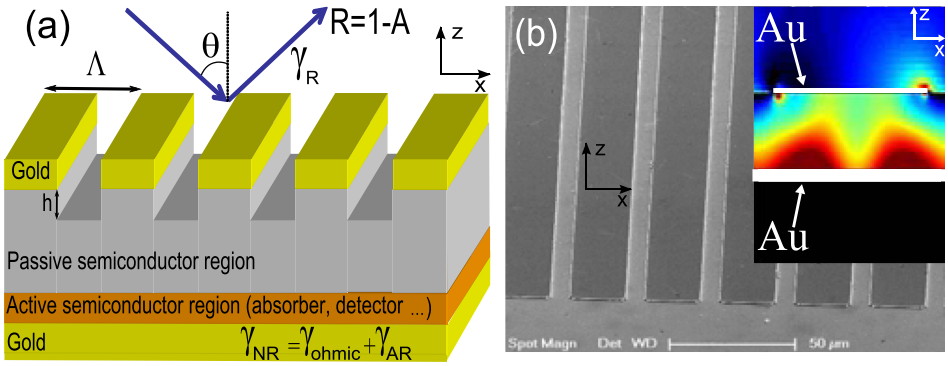

FIG. 1. (a) Schematic of the device. (b) Scanning electron micrograph of the device ($\Lambda = 30\,\mu$m, ff = 77%). The inset represents the intensity of the electric field ($|E_z|^2$) in one unit cell. The white parts represent the gold layers.

If one is able to precisely tune γ_R, it is then possible to drive the system in and out of the desired regime. In this respect, we found—using rigorous coupled wave analysis (RCWA) simulations—that the radiative loss of the resonator (γ_R) can be increased by etching the semiconductor material in between the metallic fingers, as schematically represented in Figure 1(a), where h represents the etch depth. This phenomenon can be intuitively grasped by seeing the air holes we dig in the resonator as periodically arranged radiation scattering regions, which affect γ_R. Insuring that the doping level of the n^+-GaAs layer is chosen so that it leads to non-radiative losses intrinsically higher than the radiative ones, we are then in the situation depicted in Figure 2(a): at a precise etching depth, γ_R will be equal to γ_{NR} and critical coupling will be achieved. Note that a different approach to reach critical coupling has been recently demonstrated, where the γ_{NR} of the material is tuned while γ_R is kept constant.[21]

We probed the reflectivity R(ν,θ) of such system over a large spectral bandwidth (2–7 THz at least), and a wide angular range ($13° \leq \theta \leq 67°$, Fig. 1(a)) using a Fourier transform infrared spectrometer (FTIR). Using a wire grid polarizer, the P-polarization (in the plane of incidence) of the Globar lamp beam was selected and the reflected signal was measured with a liquid-He cooled Silicon (Si) Bolometer, or with a Deuterated Triglycine Sulfate (DTGS) pyroelectric detector. The absolute reflectivity is obtained by division of the sample spectrum with a reference one from a planar gold surface. The band diagram (frequency vs in-plane wavevector) R(ν, $k_{\|}$) of a device is then readily obtained from R(ν, θ) using the relationship $k_{\|} = \frac{\omega}{c}\sin(\theta)$. The band-structure of an unetched device with $\Lambda = 30\,\mu$m and ff = 77% is shown in the left panel of Figure 3(a). The two dispersive transverse magnetic (TM) modes of the resonator are clearly observable. They are the result of the perturbation induced by the air slit of the grating, which folds the guided mode dispersion in the first Brillouin zone. At Γ-point (2nd order Bragg scattering), the photonic band-gap lies at $\simeq 2.9$ THz. At most of the incident angles, about 60% of the incoming light is coupled into the sub-wavelength system. Using an ICP reactor, we iteratively carved the sample as presented on the SEM picture of Figure 2(b). On this picture, one can easily distinguish seven successive strata of etching that occurred in-between the metallic stripes. At each step, the device band diagram was measured. The right panel of Figure 3(a) reports the experimental reflectivity R(ν, $k_{\|}$) of the same sample after an etching h = 3.25 μm. The black regions correspond to a coupling (i.e., to absorption) larger than 95%. Given the limits of the probing technique, critical coupling is reached with almost all the impinging light coupled into the system. The broadening of the full width half maximum (FWHM) of the dispersive modes (from 177 GHz to 280 GHz) constitutes a clear signature of the achieved controlled modification of γ_R. Note that the effective index of the resonator modes is modified by the semiconductor etch which explains the observed frequency blue-shift. Further etching drives the system out of the critical coupling regime and the reflectivity increases again.

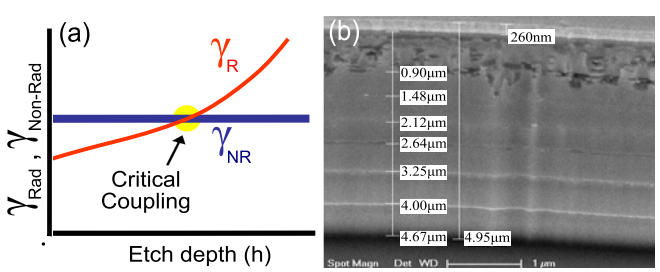

FIG. 2. (a) Schematic of the principle of critical coupling as a function of the etching depth. (b) SEM image of the device ($\Lambda = 30\,\mu$m, ff = 77%) after 7 successive etching. For each step, the measured etch depth is presented.

The experimental findings can be predicted using RCWA. The numerical details can be found in Refs. 22–25. In the present case, the SI-GaAs layer is modelled as an isotropic medium with an effective permittivity which takes into account the optical phonons contribution

$$\epsilon(\omega) = \epsilon_\infty \left(1 + \frac{\omega_L^2 - \omega_T^2}{\omega_T^2 - \omega^2 + i\omega\gamma_{ph}}\right), \quad (1)$$

where $\omega_L = 292\,\text{cm}^{-1}$, $\omega_T = 268\,\text{cm}^{-1}$, $\gamma_{ph} = 2.4\,\text{cm}^{-1}$, and $\epsilon_\infty = 11$. These values are taken from Ref. 26. The GaAs doped layer can be modelled as an isotropic dispersive medium considering the Drude contribution due to the free carriers

$$\epsilon_{dop}(\omega) = \epsilon_\infty - \left(\frac{N_{3d}e^2}{\epsilon_0 m^*\left(\omega^2 + i\frac{\omega}{\tau}\right)}\right), \quad (2)$$

where $N_{3d} = 2.6 \times 10^{18}\,\text{cm}^{-3}$ and τ (the carriers scattering time) is 0.1 ps. Finally, the dielectric function of gold is defined according to Ref. 27. Figure 3(b) reports a direct comparison between the experimental data and the curves obtained with the RCWA formalism for five different etch depths at a fixed angle of 33°. Note the logarithmic scale on

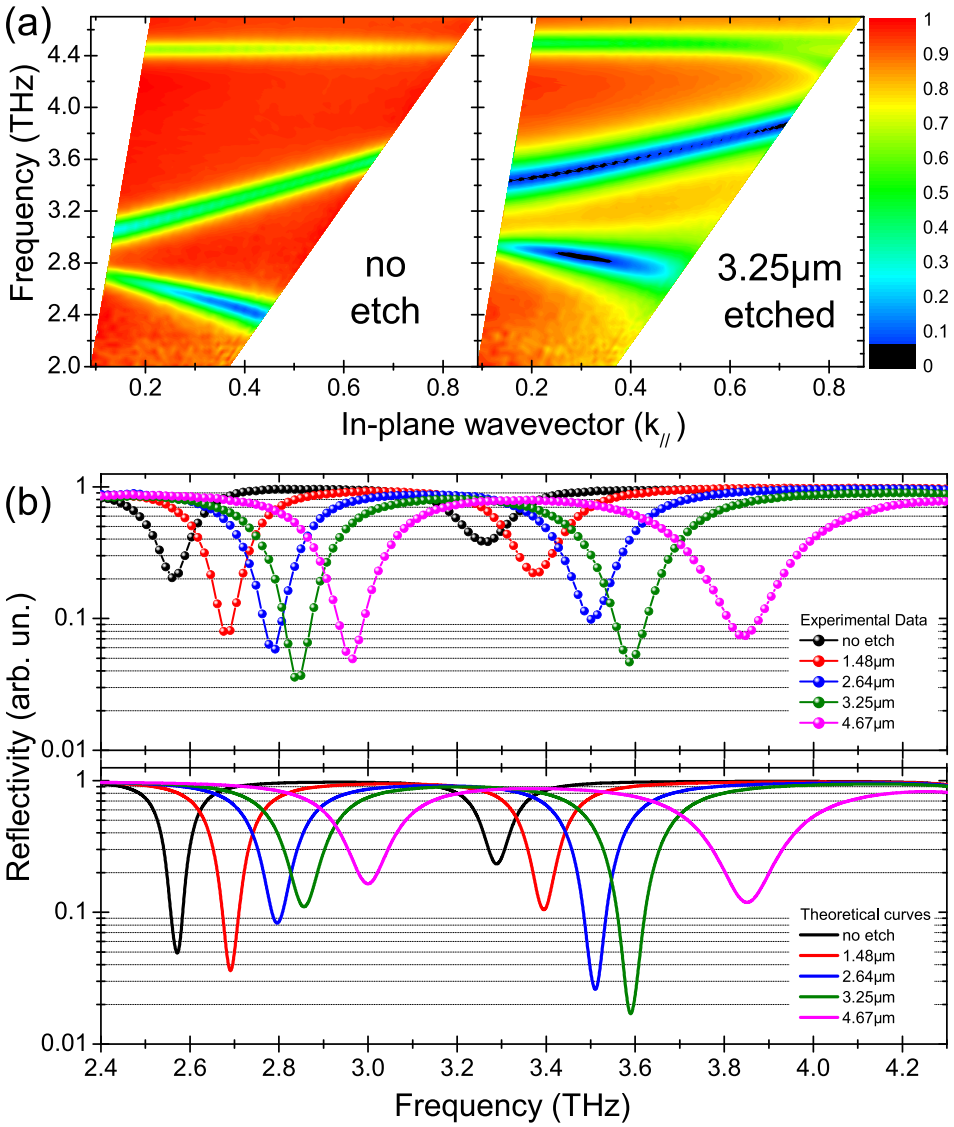

FIG. 3. (a) Experimental band diagrams of the device, before and after the etching process. The grating parameters are $\Lambda = 30\,\mu$m and ff = 77%. (b) Experimental reflectivity spectra at 33° angle (upper panel) with theoretical curves predicted from rigorous coupled wave analysis (lower panel).

the y-axis. For clarity, the data are separated in two panels (see supplementary material[28] for the overlapped curves).

First, the frequency tuning observed experimentally is remarkably well reproduced by the calculations, especially for the upper branch. Secondly, and most importantly, the levels of reflectivity and the width of the resonances are also very well reproduced for the higher dispersive branch. Similar agreements are found at other incidence angles θ. The excellent agreement between theory and experiment allows us to estimate that—at critical coupling—90% of the light is absorbed by the semiconductor active core and only 8% is dissipated in the gold. These values are very promising in view of the development of active devices.

To demonstrate the universality of this approach, we performed the same study on other samples with different filling factors, respectively, ff = 80% and ff = 73%. The controlled tuning of γ_R is observed for both samples. We will now try and plot all the data on a universal curve. According to the TCMT for a resonator coupled to an external field, the reflectivity at resonance of the one port system is described by the following expression:

$$R = \left(\frac{\gamma_R - \gamma_{NR}}{\gamma_R + \gamma_{NR}}\right)^2. \tag{3}$$

Experimentally, one has only access to the FWHM of the resonant mode representing the total loss rate $\gamma_{tot} = \gamma_R + \gamma_{NR}$. Furthermore, each sample exhibits different γ_R, γ_{NR} and consequently the expression (3) is not universal. If we now assume that the non-radiative losses remain approximately constant while etching the sample, Eq. (3) can be re-stated in terms of the total losses and the losses at the critical point as following:

$$R = \left(\frac{\gamma_{tot} - 2\gamma_{NR}}{\gamma_{tot}}\right)^2 = \left(\frac{\frac{\gamma_{tot}}{\gamma_{cc}} - \frac{2\gamma_{NR}}{\gamma_{cc}}}{\frac{\gamma_{tot}}{\gamma_{cc}}}\right)^2, \tag{4}$$

where γ_{cc} stands for the FWHM of the resonance at the critical coupling. Note that γ_{cc} is sample dependent. Since the definition of critical coupling is $\gamma_R = \gamma_{NR}$, then $\gamma_{cc} = 2\gamma_{NR}$, which leads to

$$R = \left(\frac{\frac{\gamma_{tot}}{\gamma_{cc}} - 1}{\frac{\gamma_{tot}}{\gamma_{cc}}}\right)^2. \tag{5}$$

In turn, γ_{tot} can easily be extracted from the experimental data with a Lorentzian fit (see supplementary material[28] for the

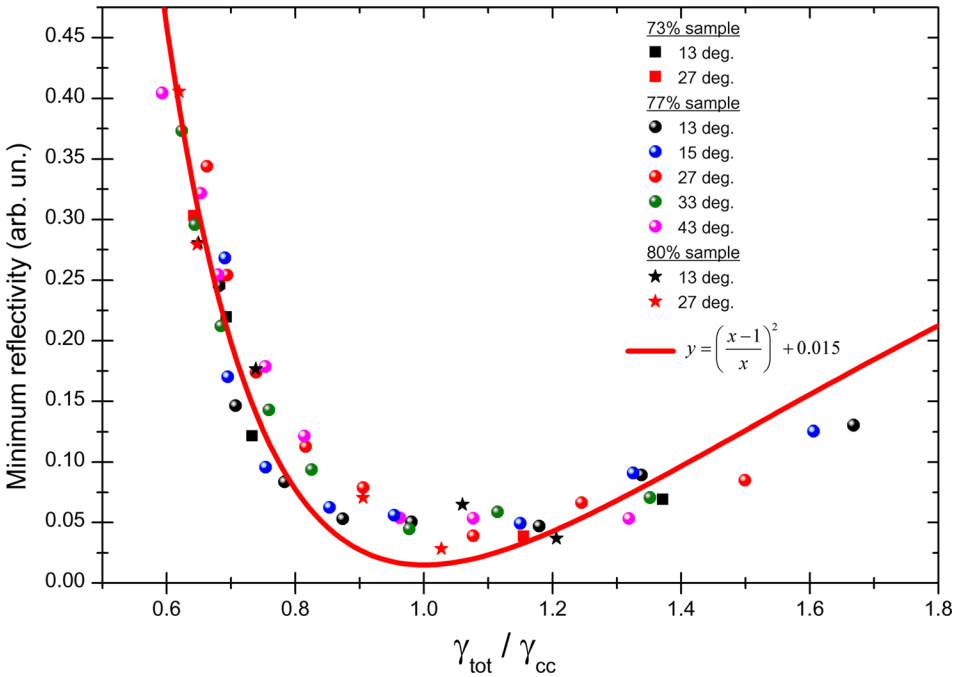

FIG. 4. Universal plot of reflectivity as function of the coupling parameter for various samples and angles.

fitting procedure). Expression (5) is universal: R is expressed as a function of the dimensionless parameter γ_{tot}/γ_{cc}.

Figure 4 shows the reflectivity at resonance for all the three samples, as a function of γ_{tot}/γ_{cc}. A very good agreement is reached between expression (5) and the experimental data. Increasing the etch depth leads to increased γ_{tot}, hence to higher values in the x-axis. The system transits from under-coupling ($\gamma_{tot}/\gamma_{cc} < 1$) to over-coupling ($\gamma_{tot}/\gamma_{cc} > 1$). When $\gamma_{tot}/\gamma_{cc} = 1$, the system is critically coupled. Note that the theoretical curve is shifted by a value of 0.015 (1.5% reflectivity) since the experimentally measured extinction ratio of the polariser is 98.5%, and a very small fraction of TE polarised radiation leaks through and shifts up the measured reflectivity. This plot is extremely practical since it gathers all the data-set onto a single curve, and it demonstrates that each single device can be brought to critical coupling via this post-processing approach. Furthermore, it allows one to directly experimentally measure γ_{rad}, which is $\frac{1}{2}\gamma_{cc}$. Finally, the universality of the curve implies that the critical coupling point can be predicted by measuring a proper number of reflectivity values before actually reaching criticality.

One could wonder if the drop in reflectivity upon etching is due to random scattering and not to absorption. On one hand, it is a very remote possibility since the reflectivity increases after reaching the critical point (Figure 4) while the radiative Q-factor keeps decreasing (see supplementary material[28] for the plot of the radiative Q-factor as a function of the etch depth). On the other hand, it is possible to perform a very elegant test to completely rule out this possibility. From blackbody theory (Kirchoff's law of thermal radiation), the radiated energy of a body in thermodynamic equilibrium is equal to the absorbed energy which reciprocally means that a better absorber is also a better thermal emitter.[29] As a corollary, the emissivity of a critically coupled device should be higher than for an unetched one. A simple test can be performed: if by heating a device which is at critical coupling more energy is collected than from a device not at critical coupling, this would undeniably prove that the light is actually coupled into the system. Two samples with quasi-same filling factors were mounted on a copper holder. One sample was etched to critical coupling while the other one was kept intact. Using the heating resistance of the cryostat, the samples were heated at 350 K and their thermal emission spectra were collected with two off-axis parabolic mirrors and re-directed into the interferometer. A polariser was used to select the polarization and the collected signal was measured with the Si Bolometer. A polarized reference signal was also measured using a bare copper mount heated to the same temperature.

Figure 5 shows a direct comparison between the emissivity of a critically coupled device (red curves) and a lower absorption device (blue curves). The polarisation is such that the electric field is orthogonal to the metallic stripes (same as the reflectivity measurements). For guidance, the reflectivity of the respective samples at $\theta = 13^\circ$ is presented in the lower panel. The correspondence between the various peaks in emission and reflection is evident. For both samples, the lower branches (non-radiative branches[30])—which are present in reflection—are quasi-non-existent in emission. This is in good agreement with the fact that the thermal signal is collected at $\theta = 0^\circ$. Furthermore, an excellent agreement is reached between the ratios of the peaks in emission and the same ratios in reflection. This result is not only aesthetically gratifying, but it proves that we have indeed tailored the light absorption in the resonator.

In conclusion, we have presented a post-processing approach which allows one to obtain optical critical coupling in highly confining THz resonators. We managed to couple more than 95% of the incoming light into a system whose thickness is ~1/10th of the wavelength. This constitutes an extremely high value for devices operating in the THz spectral range. These results appear to be highly valuable for future developments in THz physics and technology. Such cavities can for instance be employed with quantum well

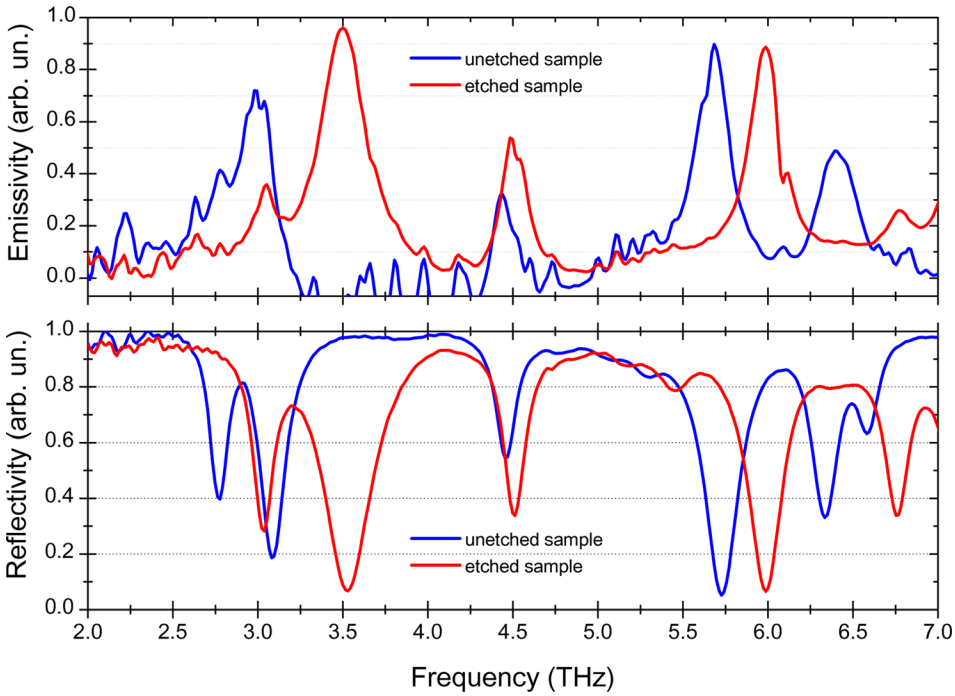

FIG. 5. Emissivity curves for the etched and unetched samples (73% ff) collected at an angle of 0°. Their respective reflectivity spectra for an angle of 13° are reported in the lower panel.

infrared THz detectors whose bandwidth is wide enough to tolerate the angular dispersion of these resonators. And the possibility of post-tuning the radiative rates is device-friendly, since these latter could be optimized after fabrication. Furthermore, this approach is valid at any wavelength upon a simple linear scaling, provided that the metallic losses do not become prohibitive.

We thank N. Isac for help with the wafer-bonding process, and J-J. Greffet for useful discussions. S.Z. acknowledges the exchange grant between Scuola Normale Superiore (Italy) and Ecole Normale Superieure (France). We acknowledge financial support from the Triangle de la Physique (Project INTENSE), and from the French National Research Agency (ANR-09-NANO-017 "HI-TEQ"). The cleanroom fabrication has been performed at the nano-center CTU-IEF-Minerve, which was partially funded by the Conseil Générale de l'Essone. This work was supported in part by the Italian Ministry of Economic Development through the ICE-CRUI project "Teragraph."

[1]H. Haus, *Waves and Fields in Optoelectronics* (Prentice-Hall, Upper Saddle River, 1984).
[2]M. Cai, O. Painter, and K. J. Vahala, Phys. Rev. Lett. **85**, 74 (2000).
[3]C. Baker, C. Belacel, A. Andronico, P. Senellart, A. Lemaitre, E. Galopin, S. Ducci, G. Leo, and I. Favero, Appl. Phys. Lett. **99**, 151117 (2011).
[4]J. T. Shen and S. H. Fan, Phys. Rev. A **82**, 021802(R) (2010).
[5]K. Vahala, *Optical Microcavities* (World Scientific Publishing, Singapore, 2004).
[6]R. M. Audet, E. H. Edwards, P. Wahl, and D. A. B. Miller, IEEE J. Quantum Electron. **48**, 198 (2012).
[7]M. Graf, G. Scalari, D. Hofstetter, J. Faist, H. Beere, E. Linfield, D. Ritchie, and G. Davies, Appl. Phys. Lett. **84**, 475 (2004).
[8]H. Luo, H. C. Liu, C. Y. Song, and Z. R. Wasilewski, Appl. Phys. Lett. **86**, 231103 (2005).
[9]G. Gomard, R. Peretti, E. Drouard, X. Meng, and C. Seassal, Opt. Express **21**, A515 (2013).
[10]H. Tao, N. I. Landy, C. M. Bingham, X. Zhang, R. D. Averitt, and W. J. Padilla, Opt. Express **16**, 7181 (2008).
[11]N. I. Landy, S. Sajuyigbe, J. J. Mock, D. R. Smith, and W. J. Padilla, Phys. Rev. Lett. **100**, 207402 (2008).
[12]N. Liu, M. Mesch, T. Weiss, M. Hentschel, and H. Giessen, Nano Lett. **10**, 2342 (2010).
[13]I. Puscasu and W. L. Schaich, Appl. Phys. Lett. **92**, 233102 (2008).
[14]J.-J. Greffet, R. Carminati, K. Joulain, J.-P. Mulet, S. Mainguy, and Y. Chen, Nature **416**, 61 (2002).
[15]X. L. Liu, T. Tyler, T. Starr, A. F. Starr, N. M. Jokerst, and W. J. Padilla, Phys. Rev. Lett. **107**, 045901 (2011).
[16]M. De Zoysa, T. Asano, K. Mochizuki, A. Oskooi, T. Inoue, and S. Noda, Nat. Photonics **6**, 535 (2012).
[17]Y. Todorov, A. M. Andrews, I. Sagnes, R. Colombelli, P. Klang, G. Strasser, and C. Sirtori, Phys. Rev. Lett. **102**, 186402 (2009).
[18]E. Strupiechonski, D. Grassani, D. Fowler, F. H. Julien, S. P. Khanna, L. Li, E. H. Linfield, A. G. Davies, A. B. Krysa, and R. Colombelli, Appl. Phys. Lett. **98**, 101101 (2011).
[19]Y. Todorov, L. Tosetto, J. Teissier, A. M. Andrews, P. Klang, R. Colombelli, I. Sagnes, G. Strasser, and C. Sirtori, Opt. Express **18**, 13886 (2010).
[20]B. S. Williams, S. Kumar, H. Callebaut, Q. Hu, and J. L. Reno, Appl. Phys. Lett. **83**, 2124 (2003).
[21]M. A. Kats, R. Blanchard, P. Genevet, and F. Capasso, Nature Mater. **12**, 20 (2013).
[22]S. Zanotto, G. Biasiol, R. Degl'Innocenti, L. Sorba, and A. Tredicucci, Appl. Phys. Lett. **97**, 231123 (2010).
[23]D. M. Whittaker and I. S. Culshaw, Phys. Rev. B **60**, 2610 (1999).
[24]L. Li, J. Opt. Soc. Am. A **13**, 1870 (1996).
[25]P. Lalanne and G. M. Morris, J. Opt. Soc. Am. A **13**, 779 (1996).
[26]E. Palik, *Handbook of Optical Constants of Solids* (Academic Press, San Diego, 1991).
[27]M. A. Ordal, L. L. Long, R. J. Bell, S. E. Bell, R. R. Bell, R. W. Alexander, and C. A. Ward, Appl. Opt. **22**, 1099 (1983).
[28]See supplementary material at http://dx.doi.org/10.1063/1.4819491 for additional information including the overlapped experimental and theoretical reflectivity curves, the fitting procedure for extraction of the total losses and the variation of the radiative Q factor as a function of the etch depth.
[29]O. D. Miller, E. Yablonovitch, and S. R. Kurtz, IEEE J. Photovoltaics **2**, 303 (2012).
[30]G. Xu, R. Colombelli, S. P. Khanna, A. Belarouci, X. Letartre, L. Li, E. H. Linfield, A. G. Davies, H. E. Beere, and D. A. Ritchie, Nat. Commun. **3**, 952 (2012).